Testing The Strong Field Dynamics of General Relativity Using Compact Binary Mergers

C. E. Fields*
School of Earth and Space Exploration, Arizona State University, Tempe, AZ

Project Mentors
T. G. F. Li, M. Isi, and A. Weinstein
LIGO Laboratory, California Institute of Technology, Pasadena, CA 91125, USA
(Dated: September 20, 2015)

Einstein's General Theory of Relativity (GR) has been well tested in the weak field regime over the past century. However, such tests have not been carried out in the highly dynamical and inherently non-linear strong field regime. Recent advancements in ground based gravitational wave detectors, (e.g., Advanced LIGO, VIRGO) will allow us to probe this regime of GR by investigating gravitational waves produced by astrophysical systems with strong gravitational fields such as compact binary coalescences. While current search techniques utilize standard GR waveforms to identify weak gravitational wave (GW) signals in the presence of noisy data, alternative theories of gravity predict signals that may differ significantly from GR. We investigate our ability to find non-GR effects in detected waveforms of an astrophysical source in an alternative theory of gravity by introducing an arbitrary parameter to modify standard GR waveform features, such as ringdown frequency, merger frequency, and amplitude. We then perform statistical methods, such as matched filtering and Bayesian inference, to quantify how well future detectors will be able to distinguish between the gravitational waveforms in the event that GR is not the final theory of gravity.

I. INTRODUCTION

General Relativity (GR) is a theory of gravity originally proposed by Albert Einstein in 1915 to generalize special relativity and Newton's law of universal gravitation. Led by the fundamental principle of equivalence, Einstein used GR to describe the motion of accelerating, massive particles by describing the associated field strength as the extent to which these particles warp the four-dimensional geometry of space and time, or *spacetime*. The principle of equivalence is now often viewed as the broader overall idea that spacetime is curved. Coupled with this fundamental postulate, [1] proposed a set of ideas which became known as the Einstein equivalence principle (EEP). Simply stated, the EEP is comprised of three broad ideas: the motion of a freely falling body under only the influence of gravity is independent of structure and composition (also known as the Weak Equivalence Principle), the outcome of any local non-gravitational experiment is independent of the velocity of the reference frame in which it is performed (local Lorentz invariance), and that the outcome of an experiment is independent of when and where it takes place in the Universe (local position invariance) [2]. The EEP has allowed for a wide range of experimental tests that aim to test the foundation of GR and the notion of curved spacetime describing the nature of gravity.

Experiments aimed at testing the foundations of GR include the perihelion shift of Mercury, the orbital decay of the Hulse-Taylor binary pulsar B1913+16, and laboratory based tests of the WEP. GR predicted the rate of perihelion shift of Mercury, $\dot{\tilde{\omega}} \sim 42.''98$ (arc seconds per century), a problem previously unsolved since announced by Le Verrier in 1859. The orbital decay of the Hulse-Taylor binary pulsar, $\dot{P}_b$, as predicted by GR yields a value of $\dot{P}_b \sim -2.402531 \pm 0.000014 \times 10^{-12}$, which matches when compared to the corrected observed value, $\dot{P}_b^{\rm corr}/\dot{P}_b^{\rm GR} \sim 0.997 \pm 0.002$ [3]. Tests of the WEP include measuring the fractional difference in acceleration between two bodies. This difference is referred to as the "Eötvös ratio" and is defined by $\eta \sim 2|a_1 - a_2|/|a_1 + a_2|$, where a_1 and a_2 refer to the acceleration of the respective bodies considered for the test. One specific example performed at the University of Washington was able to reach a value of $\eta \sim 2 \times 10^{-13}$ [4–6], with continued efforts to further constrain this parameter ongoing [7].

The strength of the gravitational field is often characterized by the "compactness" parameter, $\epsilon \sim GM/Rc^2$, where G is the gravitational constant, M is the characteristic mass, R characteristic radius, and c the speed of light in a vacuum. Despite the many successful tests of GR described here, all previous tests have been carried out in the dynamically slow and *weak* field regime. For example, within our Solar system, the field strength takes a value of $\epsilon \sim 10^{-6}$. Although many alternative theories of gravity predict solutions in agreement with GR within the weak field, they also give rise to deviations from GR in the highly dynamical and non-linear *strong* field regime.

Alternative theories of gravity that predict deviations from GR include: scalar-tensor, massive graviton, $f(R)$, variable G, non-commutative geometry and gravitational parity violation [8–14]. The parameterized post-Einsteinian (ppE) framework [15] allows one to quantify the extent to which an alternative theory

* 1; cef@asu.edu

may produce changes to the physical nature of systems in which GR is taken to be the complete theory of gravitation. For example, modified quadratic gravity predicts a change to the strong-field interaction of compact binary coalescences (CBCs) by introducing corrections to the Einstein-Hilbert action which depend on higher powers of the curvature. Such alternative theories can be tested directly by investigating these extremely relativistic and dynamical systems wherein the gravitational field strength $\epsilon \sim 0.1$ to near unity. The final moments of CBC's are extremely luminous in gravitational radiation and encoded within these gravitational wave (GW) signals is the necessary information to further constrain alternative theories of gravitation [2, 16–19].

Gravitational waves are propagating oscillations in the gravitational field caused by the acceleration of massive bodies [20]. The gravitational wave is characterized by the wave amplitude, or strain, $h \sim \Delta L/L$, where ΔL denotes the total change in length L between two objects, such as a pair of mirrors forming an optical cavity of an interferometer in the presence of gravitational radiation [19]. Carrying energy, angular momentum, and inducing orbital decay in tight compact binary systems, gravitational waves propagate unimpeded through the Universe at the speed of light. According to GR, GWs have two independent polarizations: h_+ and $h_\times$, where the distinction between the two is manifested in the way in which a circular ring of test particles in the (x, y) is affected by the presence of a transverse wave propagating in the z direction. It has been shown that GW signals can be systematically analyzed to extract intrinsic information about their astrophysical source [21–26]. Compact binary coalescences (CBCs), inspiralling binary star systems consisting of neutron stars (NSs) or black holes (BHs), are promising sources for the direct detection of gravitational wave signals for next generation gravitational wave detectors such as Advanced LIGO (aLIGO), VIRGO, and KAGRA [27–29].

Highly compact objects have field strengths that range from $\epsilon \sim 0.1$ to near unity and during the final stages of coalescence reach relativistic orbital velocities of $0.1c \lesssim v \lesssim 0.6c$, thus providing a direct probe of the highly non-linear and dynamical strong field. Beyond tests of GR, NS-NS binary systems can be used to constrain the nuclear equation of state (EOS) of ultra relativistic, degenerate neutron star matter deep within the core or to probe tidal deformations of the companion stars approaching the innermost stable circular orbit (ISCO) [30–33]. Contrary to tests on the behavior of matter in NS-NS binaries, BH-BH binaries provide the cleanest, direct test of GR as black holes are made purely of curved spacetime, allowing one to neglect the complex behavior of matter [34]. Advanced LIGO will be capable of detecting signals from these compact binary systems while also expanding the detector coverage area leading to an increase of expected detections [35–38].

The Laser Interferometer Gravitational-Wave Observatory (LIGO) project is involved in the development and operation of increasingly sensitive gravitational wave detectors. The Initial LIGO detectors were built in the late 1990's and operated at and beyond design sensitivity from 2005 to 2007 [39]. Advanced LIGO is the next generation of detectors wherein the infrastructure created with iLIGO will be upgraded and expanded to significantly increase range and detector sensitivity [35]. These upgrades are expected to give aLIGO a maximum sensitivity to strain, for a frequency band of $f \sim$ 100-200 Hz, of $h_{\rm rms} \sim 4 \times 10^{-23}$, along with an increased horizon distance of up to $\sim$ 450 Mpc. This increase in detector sensitivity also increases the number of possible events to 10-100 events per year, resulting in a higher likelihood of detection. Compact binary systems are a particularly promising candidate for direct detection of gravitational waves as well as direct tests of general relativity in the strong field regime [40].

Current techniques for determining if an observed signal originated from an astrophysical source as opposed to a non-gaussian glitch or instrumental error include checking for triggers coincident in different detectors within a small timeframe, statistically minimizing the known noise from the detector, and then using statistical methods to compare the observed signal with a template bank of approximate waveforms [41–44]. The techniques used to model the gravitational radiation emitted from different astrophysical sources, have been shown to provide an accurate description in the static slow moving, weak field regime where $v \ll c$ [45, 46]. However, alternative theories of gravity lead to GR-like solutions in the weak-field but could diverge strongly in violent events, such as the merging of two compact objects [47–49]. In the event that GR is not the complete theory of gravitation, a detection from such a highly relativistic source that emits a GW that deviates significantly from GR could bypass detection for a template bank utilizing only standard GR waveforms and also introduce unexpected degeneracies with inferred intrinsic parameters of the system. Therefore, it is proposed that the methods by which incident signals are analyzed thoroughly account for physically motivated deviations from GR that have been inferred by alternative theories of gravity.

In this paper we investigate the effect of non-GR deviations in simulated gravitational waveforms used to determine detection of a GW signal. For this investigation, we consider binary systems composed of binary black holes in the context the next generation gravitational wave detector, aLIGO. We perform numerical calculations to model these gravitational waveforms from a variety of binary systems. We then introduce a parameterized phenomenological function to modify the gravitational waveform which produces a significant deviation from GR. Then, we perform a quantitative assessment of the properties of these modified waveforms and their implications on possible detection signals. In Sect. II we discuss our methods, in Sect. III we present our standard GR waveforms, in Sect. IV we present our modified waveforms, in Sect. VII we discuss our results, and in

Sect. VIII we present our conclusions.

II. METHODS

We begin our investigation by considering briefly a first order approximation of gravitational radiation in compact binary systems. We then calculate gravitational waveforms for non-spinning, equal mass BBH systems for a range of total mass of $M \in [10, 200]\ M_\odot$ using the `IMRPhenomC` waveform approximation, an implementation within the `lalsimulation` algorithm library [50]. Once a set of standard unmodified waveforms have been constructed, we explore the effects of altering the parameters associated with our model by introducing a multiplicative parameter, $\alpha_{\rm nGR}$ used to shift the ringdown frequency. To quantify the effects of this modification on the standard waveform we perform statistical techniques such as matched filtering and Bayesian inference.

A. Compact Binary Systems

The evolution of binary systems include in order: inspiral, merger, and ringdown. The inspiral is the orbit of two bodies about a common center of mass wherein the orbital radius decreases with time due to energy loss from sources including gravitational radiation. The merger is characterized by the orbital radius below that of $a_{\rm isco}$ wherein the two bodies begin to interact whether through tidal deformation in neutron stars or direct collision. The final stage is the ringdown wherein the newly formed massive BH or NS will oscillate at a damping ringdown frequency, emitting gravitational radiation as it settles to its new state. To illustrate these systems we consider the inspiral phase of a binary black hole system in a nearly circular orbit with companion masses of $m_1 = m_2 = 5M_\odot$ and an initial orbital period of $T = 0.1$ (s).

Using Kepler's Law of Orbits, we write the relation between the orbital period and orbital separation a, for a circular orbit with $e \approx 0$,

$$\frac{T^2}{a^3} = \frac{4\pi^2}{GM}\ , \tag{1}$$

where $M = m_1 + m_2 \equiv 10\ {\rm M}_\odot$, for this example. The initial orbital velocity of the binary objects can be deduced using these values

$$v_{\rm orb} = \frac{2\pi a}{T}\ , \tag{2}$$

where the initial orbital velocities of the system considered here are an appreciable fraction of the speed of light,

$$\beta = \frac{v_{\rm orb}}{c}\ , \tag{3}$$

with $\beta \approx 0.15$ at $T = 0.1$ s. The frequency of the gravitational waves emitted for such a system can be expressed as

$$f_{\rm GW} \sim 2 f_{\rm orb}\ . \tag{4}$$

As these compact systems evolve, they rapidly spiral inwards becoming more efficient in radiating energy via gravitational waves as the orbital radius shrinks and the orbital velocities increase. We can determine the time frame in which the binary will coalesce by calculating the ISCO. We approximate its value in flat geometry as three times that of the innermost stable orbital radius as determined by the Schwarzschild solution,

$$a_{\rm isco} \sim\ 6\frac{GM}{c^2}. \tag{5}$$

The timescale in which a binary system will reach this orbit, from an initial orbital period, T, is often referred to as the "'chirp' time,

$$t_{\rm chirp} \sim \frac{5GM^2}{256\mu c^3 \beta^8}\ , \tag{6}$$

where we find, for the system considered here, $t_{\rm chirp} \approx 18.92$ (s). The approximate amplitude of the gravitational wave strain can be calculated using the stationary phase, quadrupole approximation

$$h_+(t) \sim \frac{4G^2\mu M}{Dc^4 a(t)}\cos(\Phi(t)), \tag{7}$$

where the phase can be expressed as

$$\Phi(t) \sim \int 2\pi f_{\rm GW}(t)\ dt, \tag{8}$$

where $f_{\rm GW}$ is the frequency of the emitted GW, D is the distance from the system to the observer, μ is the reduced mass $(m_1 m_2/M)$, and a is the orbital separation of two objects in a tight circular orbit. For the system here we only consider the "plus" polarization of the GW emitted. As the binary system approaches ISCO the objects orbit with orbital velocities at $\beta \approx 0.41$ and the approximate GW strain of $|h_+| \approx 2.1\times10^{-20}$ (strain) at a frequency of $f_{\rm GW} \approx 439$ Hz. The compactness of this system at ISCO yields a value of $\epsilon \sim GM/Rc^2 \sim 0.2$. The final seconds of the inspiral occur well within the non-linear, highly dynamical strong field regime providing direct tests of alternative theories of gravity that predict observable deviations from GR. The Fourier transform of the gravitational wave strain can also be useful for determining the amplitude of the GW signal in the frequency domain. We numerically compute the Fast Fourier Transform (FFT) as the following,

$$\mathcal{F}[h_+(t)] = \tilde{h}_+(f) \equiv \int_{-\infty}^{+\infty} h_+(t) e^{i2\pi f t} dt\ . \tag{9}$$

To determine the frequencies at which the gravitational wave detector will be likely to observe a detection, the incoherent sum of the various sources of the noise within

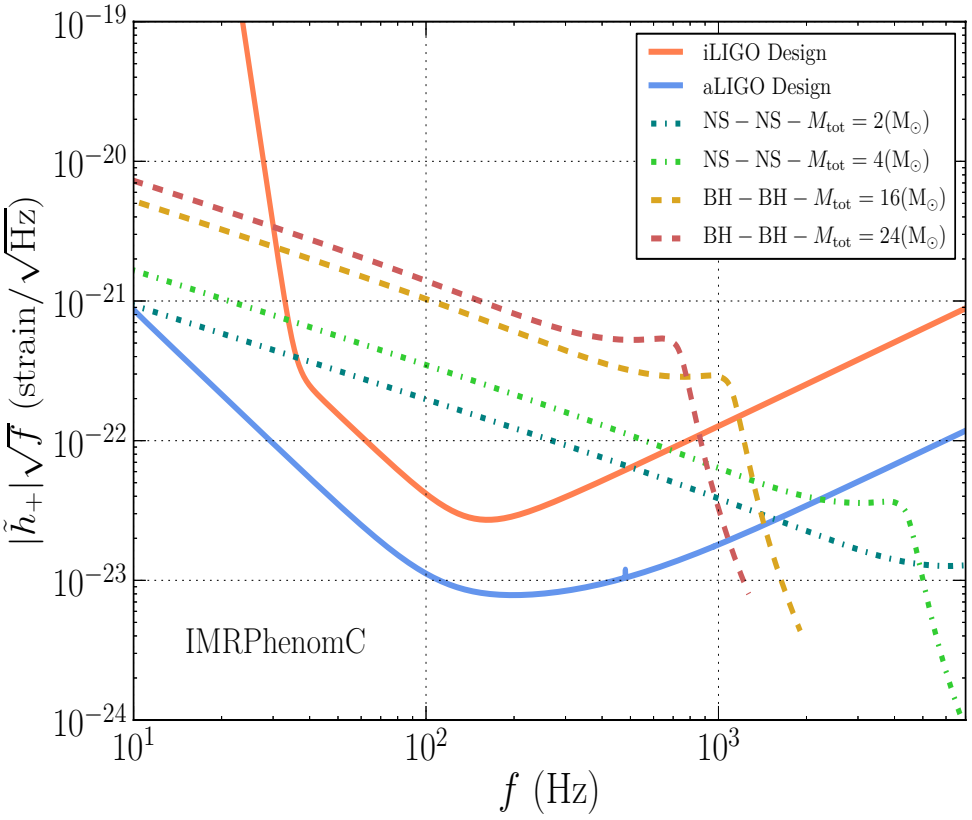

FIG. 1. Diagram showing the design amplitude spectral density of Initial LIGO (iLIGO), Advanced LIGO (aLIGO), and the equivalent gravitational wave strain for sources located at $D = 16$ Mpc with mass ratio, $q = 1$. The dark green (dash-dot) line shows a binary neutron star system (BNS) with total mass of $M_{\rm tot} \sim 2M_\odot$, while the light green (dash-dot) line shows a BNS with total mass, $M_{\rm tot} \sim 4M_\odot$. The gold (dashed) line shows a binary black hole system (BBH) with total mass of $M_{\rm tot} \sim 16M_\odot$ and the red (dashed) line shows a BBH with $M_{\rm tot} \sim 24M_\odot$.

the detector (e,g. seismic noise, thermal noise, and shot noise) are used in determining a power spectral density. The power spectral density (PSD) is the power of the noise at a given frequency, while the amplitude spectral density (ASD) can be considered as the amplitude below which the interferometer is insensitive to a detection. Therefore, it is often useful to compare the ASD of a given detector to a variety of gravitational wave signals to determine the most likely astrophysical sources. The expected amplitude spectral density for Initial LIGO (iLIGO) [39], Advanced LIGO (aLIGO) [35], and approximate GW signals from possible astrophysical sources are shown in fig. (1). The sources shown were constructed using the `IMRPhenomC` waveform approximant as described in [54] with source distances $D = 16$ (Mpc), the approximate distance to the Virgo Cluster. Figure (1) suggest that for binary neutron star systems nearing coalescence, the inspiral phase will emit gravitational radiation within the frequency band of aLIGO but the merger phase will likely occur at frequencies outside of this range. However, binary black hole (BBH) sources are predicted to experience inspiral, merger, and ringdown well within aLIGO sensitivity, such as the compact binary system considered above.

B. Modeling Gravitational Waves Emitted by Compact Binary Systems

Waveform approximations for various astrophysical sources have been constructed by combining Nth order post newtonian (PN) approximation waveforms with those calculated by the data available from numerical relativity (NR) [55–57]. `IMRPhenomC` is a phenomenological waveform model constructed using this method to describe non-precessing BBH systems [54]. These model waveforms have been shown to yield an overlap with the hybrid waveforms of greater than 97% for all BBH systems observable by Advanced LIGO and are in agreement with results obtained in [46]. For this study, we perform calculations of non-spinning, equal mass binary systems for a range of total mass using the `IMRPhenomC` template waveform as implemented in `lalsimulation`, a set of numerical routines used to compute the gravitational wave signal for a particular waveform template, contained in the `LALSuite` algorithm library [50]. Here we briefly review the steps necessary for complete and accurate waveform modeling of the BBH systems considered in this work. We focus on three aspects that completely define the GW signal, the phase, the ampli-

tude and the frequency regimes over which these models transition.

1. Phase

The first stage of compact binary coalescence is the inspiral. This stage can be adequately modeled under the assumption of a weak gravitational field using the Post Newtonian (PN) approximation to general relativity. The GW phase of the early adiabatic inspiral of a BBH coalescence is based on a stationary phase approximation and has been well modeled by the following analytical formula

$$\psi_{\rm PN}(f) = 2\pi f t_0 - \phi_0 - \frac{\pi}{4} + \frac{3}{128\eta}(\pi f)^{-5/3}\sum_{k=0}^{7}\alpha_k(\pi f)^{k/3} \ , \tag{10}$$

where f is the GW frequency, ϕ_0 is the orbital phase of the binary, and α_k corresponds to the k'th coefficient of the TaylorF2 description of the Fourier phase [58–61]. As mentioned in Section II A, the assumption that the gravitational field is sufficiently weak begins to break down as the binary approaches the pre-merger phase, $a \to a_{\rm isco}$. Modeling of the pre-merger phase, $\psi_{\rm PM}$ was done by [54] using

$$\psi_{\rm PM}(f) = \eta^{-1}(\alpha_1 f^{-5/3} + \alpha_2 f^{-1} + \alpha_3 f^{-1/3} + \alpha_4 + \alpha_5 f^{2/3} + \alpha_6 f) \tag{11}$$

where α_k are phenomenological coefficients fitted to agree with hybrid waveforms for $0.1 f_{\rm RD} \lesssim f \lesssim f_{\rm RD}$ and $\eta = \mu/M$. Lastly, the linear ansatz proposed by [54] for the ringdown phase is

$$\psi_{\rm RD} = \beta_1 + \beta_2 f \tag{12}$$

with coefficients determined by the pre-merger phase. The final phenomenological phase is produced from a smoothed transition between frequency regimes using tanh-window functions to produce

$$\Psi_{\rm IMR} = \psi_{\rm PN} w^{-}_{f_1} + \psi_{\rm PM} w^{+}_{f_1} w^{-}_{f_{\rm RD}} + \psi_{\rm RD} w^{+}_{f_{\rm RD}} \ , \tag{13}$$

where $f_1 = 0.1 f_{\rm RD}$ and $w^{\pm}_{f_1, f_{\rm RD}}$ are windowing coefficients computed to produce smooth transitions between different regimes.

2. Amplitude

The PN model of the GW amplitude obtained from the stationary phase approximation can be expressed as

$$A_{\rm PN}(f) = \mathcal{C} f^{-7/6}(1 + \sum_{i=2}^{3}\alpha_i \nu^i) \quad \text{for } f < f_{\rm isco}, \tag{14}$$

where $\nu = (\pi M f)^{1/3}$ and $\mathcal{C}$ is a numerical constant that depends on the sky location, orientation and masses [46]. While this amplitude can be considered adequate for weak gravitational fields, as the binary approaches merger, a more descriptive approach is required.

A pre-merger amplitude is proposed by the re-expansion of eqn. (14) leading to

$$A_{\rm PM} = A_{\rm PN} + \gamma_1 f^{5/3} \ , \tag{15}$$

where γ_1 is fit to obtain the pre-merger amplitude in NR simulations of binary black hole mergers [62, 63].

The ringdown amplitude is approximated using a Lorentzian

$$A_{\rm RD} = \delta_1 \mathcal{L}(f, f_{\rm RD}, \delta_2 Q) f^{-7/6} \ , \tag{16}$$

with phenomenological coefficients fit to the hybrid data. The final amplitude function, $A_{\rm phen}$ is expressed as a combination of the models given above with appropriate smoothed transitions to fully capture the entire evolution of the gravitational waveform. For a detailed review of the calculation of the fitting parameters for this phenomenological model, see Table II of [54].

3. Frequency Regimes

Possibly the most important part of construction of the phenomenological model is how one determines the frequencies at which these transitions occur. The underlying frequency that determines when these transitions occur is the BH ringdown frequency.

The ringdown frequency, $f_{\rm RD}$ is determined from the spins and masses of the black holes considered and can be computed by the following form

$$f_{\rm RD} = \frac{c^3}{2\pi G M}[k_1 + k_2(1+a)^{k_3}] \ , \tag{17}$$

where $k_{\rm i} = \{1.521, -1.1568, 0.1292\}$ while the quality factor of the BH ringdown is characterized by

$$Q_{\rm BH} = q_1 + q_2(1+a)^{q_3} \ , \tag{18}$$

with $q_{\rm i} = \{0.700, 1.4187, -0.4990\}$ as given in Table VIII of [64].The transition from pre-merger (approaching ISCO) to ringdown was chosen by [54] for a value of $f = 0.98 f_{\rm RD}$, to fit data from NR results [65].

C. Modeling Gravitational Waves Predicted by Alternative Theories of Gravity

Among the many alternative theories of gravity, only a few have been studied to the extent which observable deviations from GR can be inferred [2]. To investigate the effect of these alternatives one may consider a variety of methods. The two main methods considered are often referred to as the *top down* approach and the *bottom*

up approach. We will discuss briefly the two different approaches and their different consequences.

The *bottom up* approach involves considering a specific alternative theory and its physical influence on the system and the extent to which it will modify the GR approximation of the system. For example, Jordan-Fierz-Brans-Dicke (BD) scalar tensor theory predicts dipole radiation in addition to the quadrupole radiation predicted by GR [66–69]. The energy loss due to this radiation is expressed by

$$\dot{E}_{\rm BD} \sim -\frac{2G^3\eta^2 M^4 \mathcal{S}^2}{3c^5 a^4 \omega_{\rm BD}} \ , \tag{19}$$

where η is the symmetric mass ratio ($m_1 m_2/M^2$), M the total mass, a the orbital separation, $\omega_{\rm BD}$ is the dimensionless Dicke coupling constant and $\mathcal{S}$ is the difference in sensitivity of the two objects with sensitivity, $s_i = (\partial \ln(m_i)/\partial \ln(G))_N$ at fixed baryon number, N. The additional radiation term predicted by BD scalar tensor theory suggests that systems will be more efficient in losing the energy contained in a binary system resulting in a different cutoff frequency, $f_{\rm cut}$, than that which is predicted by GR. Therefore, one can investigate the possible consequences of a particular alternative theories and their influence on systems modeled using GR waveforms.

Alternatively, in the *top down* approach one may adopt a general framework considering deviations from GR not particular to any one alternative theory but rather adopting phenomenological parameters constrained by weak field measurements in the context of different theories. A theoretical framework for introducing such modifications to standard GR waveforms has been proposed in [15, 70]. This framework, called the "Parameterized Post-Einsteinian" (ppE) framework introduces a minimal set of parameters from which "non GR" waveforms may be constructed for the inspiral, merger, and ringdown stages of binary systems. The ppE waveform model in the stationary phase approximation is constructed by

$$\tilde{h}_{\rm nGR}(f) \sim \tilde{h}_{\rm GR}(f)[1 + \alpha u^a] e^{i\beta u^b} \ , \tag{20}$$

with

$$u \sim \pi \mathcal{M} f_{\rm GW} \ . \tag{21}$$

Eqn. (21) is the inspiral reduced GW frequency [15] and $\mathcal{M} = M\eta^{3/5}$, commonly referred to as the chirp mass. For values of $\alpha = \beta = a = b = 0$, the ppE model results in the waveform model predicted by GR. In this representation, the exponents a and b are fixed exponents for a specific modified theory of gravity, while α and β correspond to the magnitude of modification to the amplitude and phase, respectively. For example, one recovers the leading ppE corrections to the Brans-Dicke theory for $(a, \alpha, b, \beta) = (a, 0, -7/3, \beta)$ [68, 71, 72] where tracking of the Cassini spacecraft has provided constraints on the parameters, α and β [73].

D. Matched Filtering

Proper analysis of a gravitational wave signal requires the ability to determine as much about the astrophysical source as possible. One such technique used for estimating the parameters of a given GW signal is known as matched filtering. Matched filtering is a technique in which a GW signal can be analyzed to determine how well it correlates or *matches* a template waveform for a particular set of intrinsic input parameters. A match threshold may be set such that a time series, $s(t)$, must match with a particular waveform by more than, say, 97%. To calculate the match of a GW signal and a particular waveform we first determine the the overlap, using the following noise weighted inner product

$$\langle A|B\rangle = 4\Re \int_{-\infty}^{+\infty} \frac{\widetilde{A}(f)\widetilde{B}^*(f)}{S_n(f)} df \ , \tag{22}$$

where $S_{\rm n}$ is the power spectral density of the detector, $\tilde{A}$ is the FFT of a signal A, and $\tilde{B}^*$ is the complex conjugate of the FFT of a waveform template B. The optimal signal to noise ratio (SNR,ρ) of the filter is

$$\rho^2_{\rm opt} = \langle A|A\rangle \ , \tag{23}$$

and the normalized match can then be calculated by maximizing the overlap for ϕ_0 and t_0,

$$\text{Match} = \max_{\{\phi_0, t_0\}} \frac{\langle \text{A}|\text{B}\rangle}{\sqrt{\langle \text{A}|\text{A}\rangle \langle \text{B}|\text{B}\rangle}} \ . \tag{24}$$

For a given signal A, such that $A \approx B$, the match will yield a value of unity, matching the template waveform to 100%. Matched filtering allows for a quantitative assessment of the differences between signals and template waveforms as well as a means by which non GR deviations to the waveform approximations can affect the match. In addition to t_0 and ϕ_0, signals are identified by maximizing the match over other parameters such as the component mass, spins, etc.

E. Bayesian Inference

Statistical methods have been applied to the analysis of weak gravitational wave signals in the presence of noisy data to: (i) Test competing hypotheses through the computation of the evidences, or marginal likelihoods, of different models, and (ii) estimate parameters of a particular signal. [74–80]. The former is often referred to as *model selection* and is used to quantify our ability to distinguish between different models, or theories of gravity, while the latter (*parameter estimation*) is concerned with the ability to infer parameters using a GW signal within a particular theory of gravity or a particular parameterization of ppE parameters, such as those discussed in section II C. Here we describe these techniques within the

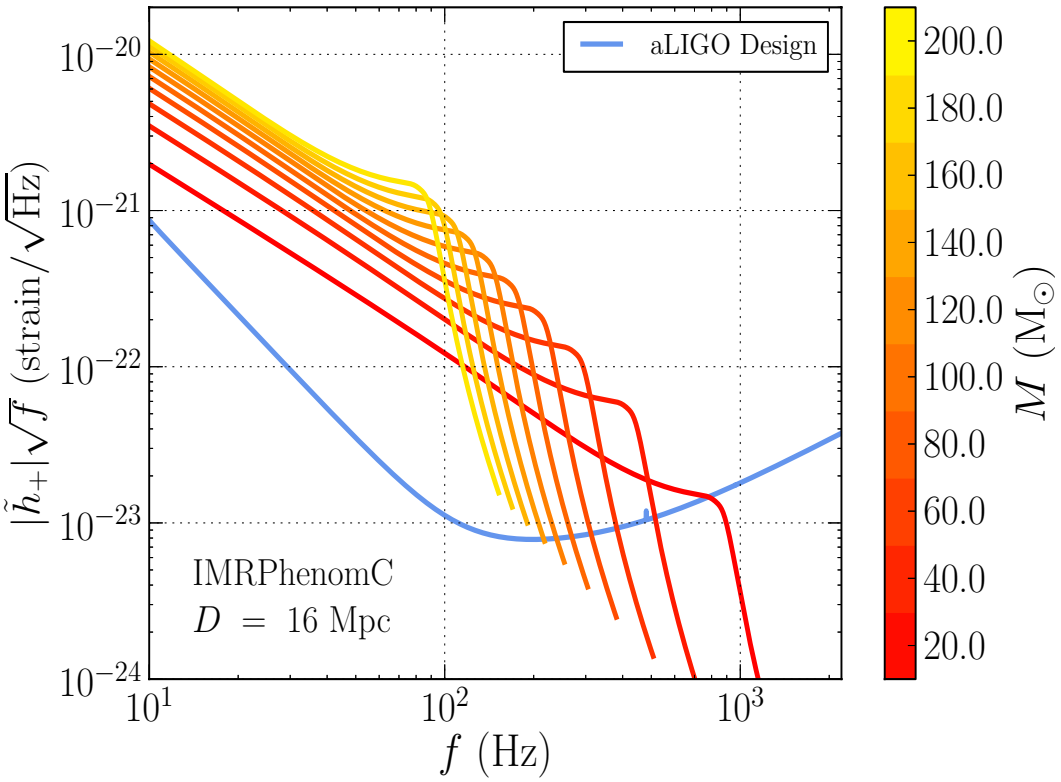

FIG. 2. Diagram showing the inspiral, merger, and ringdown gravitational wave strain as a function of frequency for a set of different systems. The waveform template used for these calculations was `IMRPhenomC`, a phenomenological waveform template constructed to describe non-precessing binary black hole systems. The systems considered here were equal mass, non spinning, $\chi = 0$, and were of the mass range $M \in [20, 200]\ M_\odot$, a range chosen to encompass low to intermediate mass BH binaries. The most massive binaries, those with $M \geq 160\ M_\odot$, merge before $f_{\rm GW} \sim 100$ (Hz) while the less massive systems take longer to merge, with merger frequency increasing as total mass decreases.

context of Bayesian inference and as an application to non-GR waveform analysis with aLIGO.

We wish to compute the posterior probability of a particular value of $\alpha_{\rm nGR}$, given a set of data, d and backgroud information I. The set of parameters considered is $\vec{\mathbf{X}} = \{\ldots, \chi, q, D, z, \phi_0\}$. To determine the posterior, we first compute the evidence, $P(d|\alpha_{\rm nGR}, I)$, by

$$P(d|\alpha_{\rm nGR}, I) = \int d\vec{\mathbf{X}} p(\vec{\mathbf{X}}|I) p(d|\alpha_{\rm nGR}, \vec{\mathbf{X}}, I)\ , \qquad (25)$$

where $p(\vec{\mathbf{X}}|I)$ is the prior probability for the parameters and $p(d|\alpha_{\rm nGR}, \vec{\mathbf{X}}, I)$ is the likelihood density distribution. By a straightforward application of Bayes' theorem we can then calculate the posterior probability distribution of our non-GR parameter by

$$P(\alpha_{\rm nGR}|d) = \frac{P(d|\alpha_{\rm nGR}, I) P(\alpha_{\rm nGR}|I)}{P(d|I)}\ , \qquad (26)$$

yielding the normalized posterior, marginalized over the additional parameters $\vec{\mathbf{X}}$. For the purpose of this study we restrict our parameter space to consider only the total mass of the system. The remaining intrinsic parameters of the system, such as $\mathcal{M}, \chi, q, D, z$, and ϕ_0 are shown in Table (I) and chosen to provide a baseline model against which we can compare. To estimate this posterior probability distribution we used a Markov chain Monte-Carlo (MCMC) simulation implemented within `lalinference`, a set of Bayesian statistical methods for use in GW data analysis. For a detailed review of the MCMC implementation, see [81].

III. STANDARD GR WAVEFORMS

To begin our investigation, we first consider a set of standard waveforms as predicted by GR. The waveform template considered is the `IMRPhenomC` model [46]. We use this template to compute the inspiral, merger, and ringdown phase of binary BH systems in the mass of $M \in [20, 200]\ M_\odot$. To compute this GW signal requires a choice of input parameters corresponding to intrinsic parameters of the astrophysical source. These parameters include the orbital phase of the binary system, the frequency interval (sampling rate), the BH reduced mass spin parameter χ, starting and stopping frequencies, and

lastly, the distance from the source. We wish to study deviations from GR that could potentially manifest themselves as very small changes to the overall waveform. Therefore, it is important that one not introduce unnecessary uncertainty to the system by an impractical choice of input parameters [81–83].

TABLE I. Input Parameters

Parameter	Value
Orbital Phase (ϕ_o)	0 (rad)
Frequency Interval (Δf)	1/32 (Hz)
Reduced Mass Spin (χ)	0.0
Mass Ratio (q)	1
Start Frequency ($f_{\rm min}$)	10 (Hz)
End Frequency ($f_{\rm max}$)	4,000 (Hz)
Distance (D)	16 (Mpc)

We restrict our investigation to non-spinning, BBH systems at the peak orbital phase and at a relatively close distance. The frequency interval, or sampling rate, of the calculation is arbitrary except in that we require it be sufficiently resolved to properly compute the waveform. The component masses considered are equivalent to half of the total mass for a mass ratio of $q = m_1/m_2 = 1$. The computation interval, the start and ending frequencies, were chosen such that the entire evolution of the system was calculated for frequencies detectable by aLIGO, $f_{\rm min} \geq 10$ Hz. The standard input parameters used throughout this paper are shown in Table (I) provide a baseline set of waveforms with which we can compare. Figure (2) shows the inspiral, merger, and ringdown gravitational wave strain in the frequency domain for a grid of models from total mass, M from $M \leq 10 \leq 200 M_\odot$. We can see that the most massive BBH systems ($M \geq M = 160\ M_\odot$), the merger occurs at a GW frequency of $f_{\rm GW} \sim 100$ Hz. This frequency corresponds to the approximate frequency at which aLIGO is designed to be most sensitive (see fig. 1). The mass range considered for this study may not represent the most likely mass range of binary black hole systems in nature but allows for a first step towards quantifying the effects of non-GR deviations using potential astrophysical sources. See [84, 85] for a review of potential candidates of BBH systems and the associated population characteristics.

IV. MODIFIED WAVEFORMS

Here we introduce our method to implement deviations from general relativity that may have non-negligible effects on the gravitational waveform used in detection of GW signals. We focus our investigation by considering only the `IMRPhenomC` waveform and discuss the associated parameters and our motivation in altering this waveform. The SNR lost by introducing these deviations is examined to determine our ability to detect gravitational waves by using waveform templates predicted by general relativity. To explore potential deviations from GR that may arise in highly dynamical and non-linear systems, we consider physical quantities used in the construction of the phenomenological models for template waveforms.

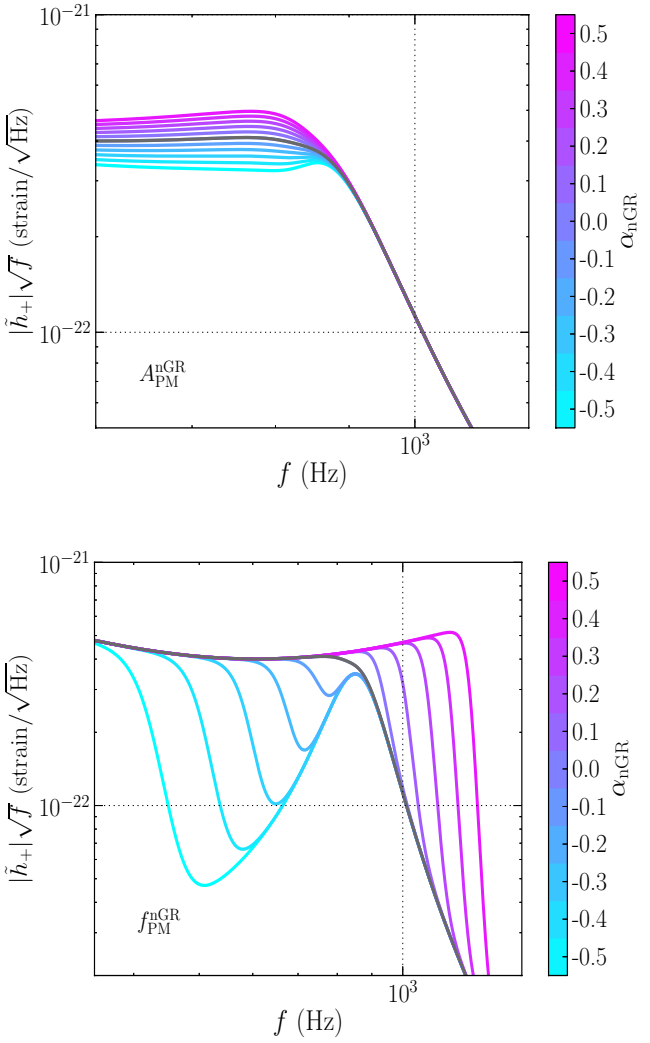

FIG. 3. Diagrams showing the inspiral, merger, and ringdown evolution of a BBH system with total mass $M = 20$ M$_\odot$ using the standard input parameters listed in Table (I). The modified waveforms use a value of $\alpha_{\rm nGR} \in [-0.5, 0.5]$ to alter the pre-merger amplitude $A_{\rm PM}^{\rm nGR}$ (top) and the pre-merger frequency $f_{\rm PM}^{\rm nGR}$ (bottom). The (gray) line shown is each diagram represents the standard GR waveform for $\alpha_{\rm nGR} = 0$.

To begin, let ψ_i be a physical parameter of the phenomenological waveform contained in the set of all pa-

rameters such that

$$\vec{\Psi} = \bigotimes_{i=0}^{N} \{\psi_i\} \tag{27}$$

We can then perform generic modifications to a particular parameter by adding a deviation, $\alpha_{\rm nGR}$, in the following way:

$$\psi_i^{\rm nGR} = \psi_i^{\rm GR}[1 + \alpha_{\rm nGR}] \ , \tag{28}$$

allowing us to investigate one parameter at a time. With the intention of investigating the strong field dynamics of GR, we focus on modifications to the pre-merger and ringdown phase. For all of the modifications considered here we use values of $-0.5 \lesssim \alpha_{\rm nGR} \lesssim 0.5$, to represent a small deviation from GR.

A. Pre-Merger

We first modify the amplitude of the pre-merger in the `IMRPhenomC` waveform template using eqn. (28). The GW strain for this modification for a range of values is shown in (top panel) Figure (3). The color bar shown represents a discrete value of $\alpha_{\rm nGR}$ used to generate the waveform. Also shown in each panel is the standard waveform predicted by GR (gray line) for $\alpha_{\rm nGR} = 0$. The pre-merger regime is of particular interest since it is well within the strong field and the velocities of the companions as are extremely relativistic (see Sec. II A). Also shown in Figure (3) (bottom panel) is the GW strain for a set of waveforms for which the pre-merger frequency, $f_{\rm PM}$, was modified. We can see that for $\alpha_{\rm nGR} \sim \pm 0.1$, the waveform is shifted dramatically. Such modifications can lead to a significant loss in SNR ratio for GW searches which utilize standard GR waveforms, the extent of this effect is discussed in Sec. (V).

B. Ringdown

Next, we consider the ringdown amplitude in the `IMRPhenomC` waveform template. Defined in eqn. (16), the ringdown amplitude $A_{\rm RD}$ is modified using eqn. (28). Figure (4) (top panel) shows this alteration of the waveform. Modification of the frequency at which the ringdown occurs, $f_{\rm RD}$, is shown in (bottom panel) fig. (4). The modification to this parameter is represented by a monotonic shift in the waveform, which could be due to a system in which the binary is more efficient in radiating away energy than as predicted by GR. This could lead to the system reaching ISCO, or merging sooner than anticipated.

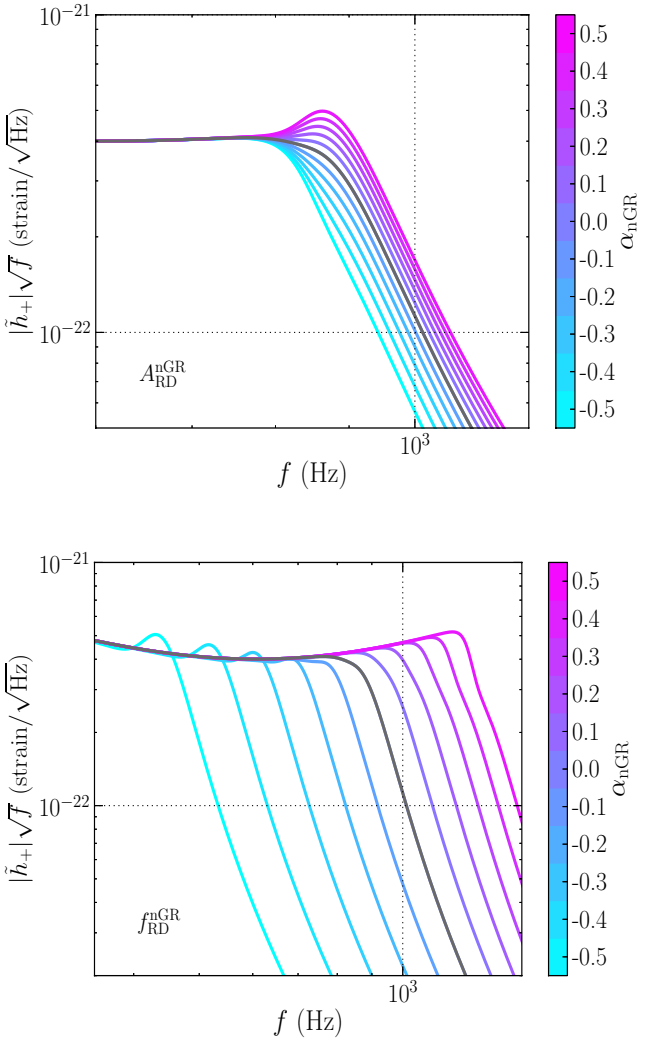

FIG. 4. Diagrams showing the inspiral, merger, and ringdown evolution of a BBH system with total mass $M = 20(\rm M_\odot)$ using the standard input parameters listed in Table (I). The modified waveforms use a value of $\alpha_{\rm nGR} \in [-0.5, 0.5]$ to alter the ringdown amplitude $A_{\rm RD}^{\rm nGR}$ (top) and the ringdown frequency $f_{\rm RD}^{\rm nGR}$ (bottom). The (gray) line shown is each diagram represents the standard GR waveform for $\alpha_{\rm nGR} = 0$.

V. OVERLAP STUDIES

We now focus our attention on quantifying the extent to which these non-GR modifications affect next generation gravitational wave detectors, specifically, aLIGO. We perform matched filtering techniques on a set of modified waveforms to address this question. Figure (5) shows the match calculated for a range of total system masses such that $M \in [20, 200]\ M_\odot$. The values of $\alpha_{\rm nGR}$ considered were chosen such that $\alpha_{\rm nGR}$ ranges from -0.5 to 0.5, where $\alpha_{\rm nGR} = 0.0$ is the standard GR waveform, such as those shown in fig. (2).

We find that, in general, modifications to the pre-merger and ringdown amplitudes do not result in a large loss in match. The loss in match can be considered as a probe for how steeply the SNR is affected by these modifications, because of the relationship shown in eq. (24),

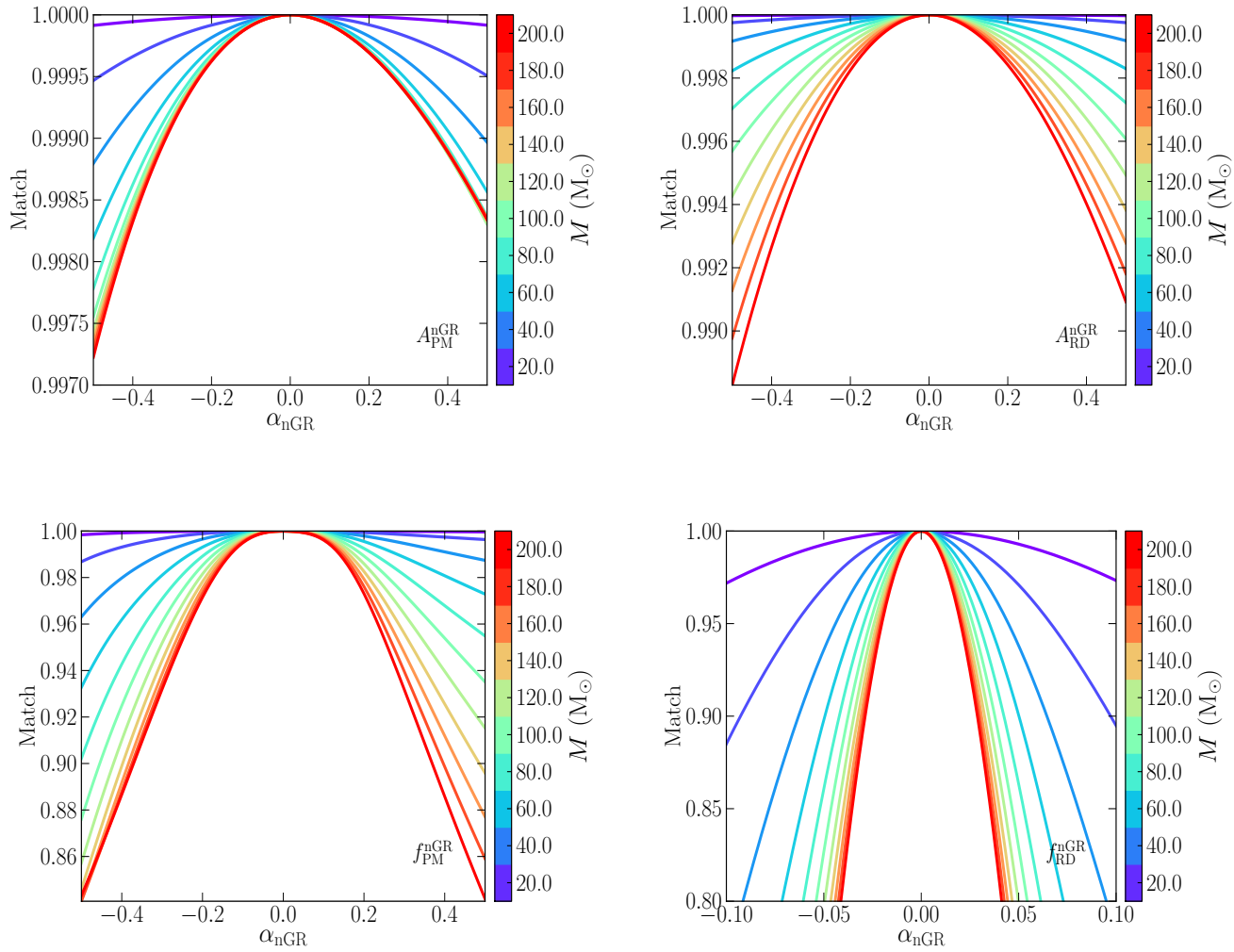

FIG. 5. Match calculations for a range of total system masses from 20 $M_\odot$ to 200 $M_\odot$ for modifications to the pre-merger amplitude (top-left), ringdown amplitude (top-right), pre-merger frequency (bottom-left), and ringdown frequency (bottom-right). The calculations used parameters listed in Table (I).

Match $\propto$ ρ. For example, in fig. (5) we see that for even the largest modification considered ($\alpha_{\rm nGR} = \pm 0.5$) the match yielded falls by $\sim 0.3\%$ from a value of unity obtained with the standard GR waveform for the pre-merger amplitude (top-left panel) and by $\sim$ 0.1% for the ringdown amplitude (top-right panel). However, for the same modification values considered we see that the pre-merger and ringdown frequencies are much more sensitive to deviations. In fig. (5) we see the match for the pre-merger frequency falls by $\sim 15\%$ for $\alpha_{\rm nGR} \pm 0.5$ and total mass $M = 200\ M_\odot$. For lower mass systems (e.g., $M = 60\ M_\odot$), the loss in match in much steeper when modifying the ringdown frequency (bottom-right panel) in fig. (5), with the match falling by $\sim 20\%$ from unity. Such a feature could arise from the aLIGO design sensitivity ASD used in the calculations. A value of $\alpha_{\rm nGR} = -0.1$ will result in a shift of the waveform towards a region in which their is a larger SNR value, making it easier to identify non-GR features.

VI. PARAMETER ESTIMATION

An important step in analyzing GW data is the ability to estimate the parameters of the astrophysical source form which the detection originated. To quantify our ability to recover injected parameters form weak GW signals in the presence of noisy data, we use a nested sampling MCMC algorithm within `lalinference`. Given some data d, we wish to understand how well we can estimate parameters using standard GR waveform templates with the increased aLIGO design ASD. Additionally, we look to explore the difference in parameter recovery when using modified waveforms. We outline the input param-

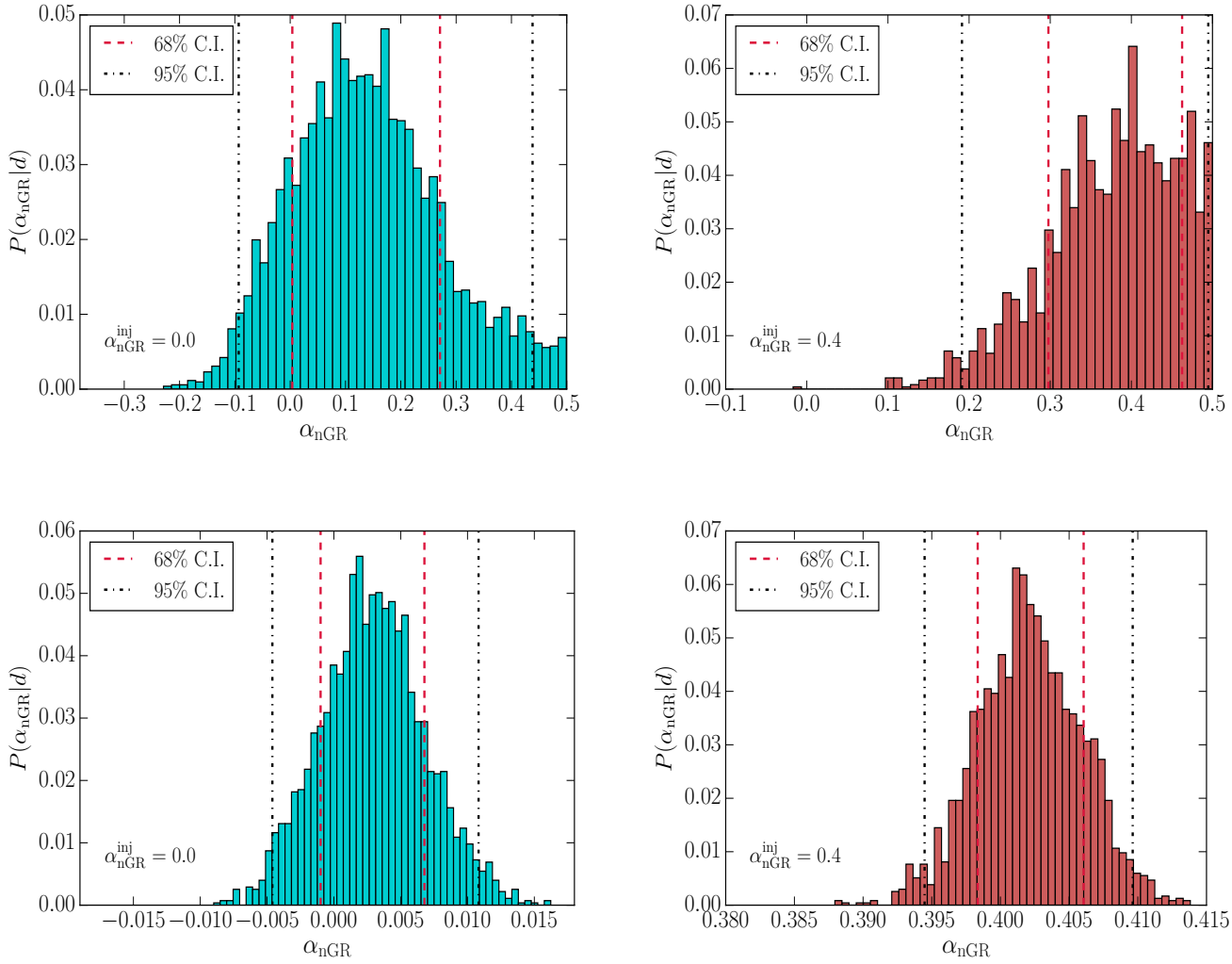

FIG. 6. Posterior distribution of $\alpha_{\rm nGR}$ given the data d for a set of pinned parameters and an injected value of $\alpha_{\rm nGR} = 0.0$ (left panels) and $\alpha_{\rm nGR} = 0.4$ (right panels). The 68% confident interval is shown by the (dashed-red) lines while the 95% confident interval is shown by the (dashed-black) lines. The injected chirp mass for the low mass system (top panels) was $\mathcal{M} \sim 8.65\ M_\odot$ and $M = 20 M_\odot$, with a source distance of $D = 99.95$ Mpc, and SNR ~ 24. While the injected chirp mass for the high mass system (bottom panels) was $\mathcal{M} \sim 86.99\ M_\odot$ and $M = 200 M_\odot$, with a source distance of $D = 112.95$ Mpc, and SNR ~ 174.

eters used for our MCMC calculations in tbl. (II). This section will focus on modifications to only the ringdown frequency as described in sec. (IV B).

We perform four `lalinference` calculations using $\alpha_{\rm nGR} = 0.0$ for $\mathcal{M} \sim 8.65\ M_\odot$ (hereafter "low-mass"), and $\mathcal{M} \sim 86.99\ M_\odot$ (hereafter "high-mass") then repeat the calculations using $\alpha_{\rm nGR} = 0.4$. In fig. (6) we show the posterior probability distribution for a MCMC calculation utilizing the prior information outlined in tbl. (II). The (top-left) panel shows the low mass calculation for which $\alpha_{\rm nGR}^{\rm inj} = 0.0$. The 68% confident interval is shown by the (dashed-red) lines while the 95% confident interval is shown by the (dashed-black) lines. This provides a baseline against which we can expect to be able

TABLE II. `lalinference` Priors

Parameter	Value
Live Points ($N_{\rm live}$)	$N_{\rm live} \geq 512$
Distance (D)	99.8529205 (Mpc)
Orbital Phase ($\phi_{\rm o}$)	0.0
Coalescence Phase ($\phi_{\rm c}$)	2.395998
Lower Frequency ($f_{\rm low}$)	10 (Hz)
Detectors	L1,H1
Power Spectral Density ($S_{\rm aLIGO}$)	`aLIGO_DESIGN`

to measure our new non-GR parameter $\alpha_{\rm nGR}$. We see that although we have not introduced a modification to our waveform here, our 95% confidence interval spans a value of $-0.1 \lesssim \alpha_{\rm nGR} \lesssim 0.44$ for a fixed chirp mass of $\mathcal{M} \sim 8.65\ M_\odot$ and an SNR of 23.3. For $\alpha^{\rm inj}_{\rm nGR} = 0.4$ (top-right panel), we see a similar distribution with a peak near the injected value. While we see that the distributions tend towards the injected values, we see a broad range for our 95% confidence intervals (C.I.), $\Delta\alpha \sim 0.52$ for $\alpha^{\rm inj}_{\rm nGR} = 0.0$ and $\Delta\alpha \sim 0.3$ for $\alpha^{\rm inj}_{\rm nGR} = 0.4$. The smaller range for $\alpha_{\rm nGR} = 0.4$ is likely due to that in our numerical implementation, we limit our study to values of $\alpha_{\rm nGR} \in [-0.5, 0.5]$. If the sampler were able to attempt values beyond 0.5, we would expect a similar width for our low mass $\alpha^{\rm inj}_{\rm nGR} = 0.0$ posterior distribution. The offset in the posterior distribution in (left panel) fig. (6) is likely due to the ASD used in the calculations. For positive values of $\alpha_{\rm nGR}$, the waveform may be shifted to less SNR, making it difficult to distinguish our non-GR modifications. Conversely, a waveform may be shifted towards higher SNR for negative values of $\alpha_{\rm nGR}$ making it easier to estimate the injected value. Therefore, we see an offset in our posterior distribution even for $\alpha_{\rm nGR} = 0.0$ due to the non-linear nature of the ASD as well as the loss of SNR due to shifts in the waveform caused by our non-GR parameter.

In stark contrast to our ability to measure $\alpha_{\rm nGR}$ for relatively low mass BBH systems, we show the posterior probability for a higher mass system in fig. (6) (bottom panels). Similar to the low mass systems, the parameters utilized initialization values enumerated in tbl. (II). In the (bottom-left panel) of fig. (6) we see the posterior probability for an injected value of $\alpha^{\rm inj}_{\rm nGR} = 0.0$. The 68% confidence interval region is shown by the (red-dashed) vertical lines. We see that higher mass systems we can provide a much stronger constraint on measurements performed on our non-GR. This distribution suggests that with 98% confidence, we can assume that $\alpha_{\rm nGR}$ lies with -0.004 and 0.011. For $\alpha^{\rm inj}_{\rm nGR} = 0.4$, fig. (6) bottom-right panel, we see a similar trend. The posterior spans a narrow range about the injected value, allowing us to claim with 95% confidence $\alpha_{\rm nGR}$ is between 0.394 to 0.409. The increase in our ability to measure such small deviations of standard GR waveforms in high mass systems can be directly attributed to the increase in SNR for these systems. The increase in mass shifts the waveform higher into the aLIGO sensitivity curve, e.g., the 200 $M_\odot$ system in fig. (2). The range of the 95% confidence intervals for high mass systems is significantly less than those for low mass. With $\alpha_{\rm nGR} = 0.0$, we find $\Delta\alpha \sim 0.015$ and for $\alpha_{\rm nGR} = 0.4$ we also find $\Delta\alpha \sim 0.015$.

VII. DISCUSSION

We have investigated modifications to the phenomenological waveform template `IMRPhenomC` by introducing a multiplicative parameter $\alpha_{\rm nGR}$ to different physical parameters used in the construction of the complete inspiral-merger-ringdown evolution of binary black hole systems. For these modified waveforms we have performed overlap studies for a range of total mass systems between 20 $M_\odot$ to 200 $M_\odot$. Furthermore, we have computed the posterior probability distribution for modifications to the ringdown frequency using the ASD for the expected aLIGO GW detector. We now compare our results with previous efforts and discuss implications for next generation GW detectors.

Work by Agathos et al. [18] found that a GR violation of as small as 10% in the inspiral phase of BNS systems, can be distinguished in BNS systems to nearly 100%. They used similar statistical methods including the odds ratio calculated within the Bayesian framework. With as few as 15 sources, they show that one can separate an event in which a 10% modification to the `TaylorF2` at 1.5PN order. While our results agree with the ability to strongly distinguish between GR and non-GR sources for high mass BBH systems, we do not reach such precision for our low mass systems. However, if our calculations were carried out on multiple sources such as in [18], we may find that a more stringent constraint can be placed on $\alpha_{\rm nGR}$ using low mass BBH mergers. Furthermore, we consider less parameters for our investigation that could impact this result e.g. detector calibration, spin, etc.

VIII. CONCLUSION AND FUTURE WORK

We have shown that high mass BBH systems are efficient in detecting small deviations from GW waveforms as predicted by GR. Deviations form GR can be measured with 98% confidence from $\sim$ -0.005 to 0.01 of its standard GR value using waveform templates to simulate the inspiral, merger, and ringdown of BBH systems. This result suggests that next generation GW detectors such as Advanced LIGO can measure such deviations to high precision. Furthermore, we find that low mass systems are not as efficient in distinguishing small deviations from GR, but provide a C.I. range that can be used with other analysis methods to reach a precision as those for the higher mass systems.

Future work includes using the methods described here different waveforms and additional intrinsic parameters not considered here e.g. spin, mass ratio, source distance, etc. Additionally, one should investigate the degeneracies that arise by introducing a generic modification to the standard waveform. For example, a value of $\alpha_{\rm nGR} = 0.1$ applied to modify the ringdown frequency could shift the waveform in the frequency domain such that although we know a priori, the total mass $M = 20\ M_\odot$, the deviation causes the recovered total mass to be larger e.g. $M = 20 \pm 2\ M_\odot$. The method should also be extended to allow generic modifications to arbitrary waveform parameters found in other templates such as `TaylorF2, IMRPhenomD, SpinTaylorT4` etc. Lastly, a rigorous framework should then be im-

plemented with the GW analysis package `lalsuite` to allow for further study and robust parameter estimation studies beyond GR.

ACKNOWLEDGMENTS

C.E.F. thanks A.W.,T.L., and M.I. for their guidance and mentorship through a very successful and rewarding summer. C.E.F. also acknowledges Johnathon Lowery for many insightful discussions and fellow SURF colleagues for their advice and companionship. This project was supported by the National Science Foundation, California Institute of Technology under the 2015 LIGO Summer Undergraduate Research Fellowship, and the National Society of Black Physicists under the Carl A. Rouse Fellowship. We are grateful for computational resources provided by the Leonard E Parker Center for Gravitation, Cosmology and Astrophysics at University of Wisconsin-Milwaukee.

[1] R. H. Dicke, in *Relativity, Groups and Topology. Relativité, Groupes et Topologie*, edited by C. M. DeWitt and B. S. DeWitt (Gordon and Breach, New York; London, 1964) pp. 165–313.
[2] C. M. Will, Living Reviews in Relativity **17**, 4 (2014), arXiv:1403.7377 [gr-qc].
[3] J. M. Weisberg, D. J. Nice, and J. H. Taylor, Astrophys. J. **722**, 1030 (2010), arXiv:1011.0718 [astro-ph.GA].
[4] E. G. Adelberger, Classical and Quantum Gravity **18**, 2397 (2001).
[5] S. Schlamminger, K.-Y. Choi, T. A. Wagner, J. H. Gundlach, and E. G. Adelberger, Physical Review Letters **100**, 041101 (2008), arXiv:0712.0607 [gr-qc].
[6] T. A. Wagner, S. Schlamminger, J. H. Gundlach, and E. G. Adelberger, Classical and Quantum Gravity **29**, 184002 (2012), arXiv:1207.2442 [gr-qc].
[7] C. C. Speake and C. M. Will, Classical and Quantum Gravity **29**, 180301 (2012).
[8] C. Brans and R. H. Dicke, Physical Review **124**, 925 (1961).
[9] T. Damour and G. Esposito-Farese, Classical and Quantum Gravity **9**, 2093 (1992).
[10] K. Hinterbichler, Reviews of Modern Physics **84**, 671 (2012), arXiv:1105.3735 [hep-th].
[11] E. A. Bergshoeff, O. Hohm, and P. K. Townsend, Physical Review Letters **102**, 201301 (2009), arXiv:0901.1766 [hep-th].
[12] N. Yunes and L. C. Stein, Phys. Rev. D **83**, 104002 (2011), arXiv:1101.2921 [gr-qc].
[13] K. Yagi, L. C. Stein, N. Yunes, and T. Tanaka, Phys. Rev. D **85**, 064022 (2012), arXiv:1110.5950 [gr-qc].
[14] A. V. Frolov and J.-Q. Guo, ArXiv e-prints (2011), arXiv:1101.4995 [astro-ph.CO].
[15] N. Yunes and F. Pretorius, Phys. Rev. D **80**, 122003 (2009), arXiv:0909.3328 [gr-qc].
[16] R. N. Lang, Phys. Rev. D **91**, 084027 (2015), arXiv:1411.3073 [gr-qc].
[17] W. Del Pozzo, K. Grover, I. Mandel, and A. Vecchio, Classical and Quantum Gravity **31**, 205006 (2014), arXiv:1408.2356 [gr-qc].
[18] M. Agathos, W. Del Pozzo, T. G. F. Li, C. Van Den Broeck, J. Veitch, and S. Vitale, Phys. Rev. D **89**, 082001 (2014), arXiv:1311.0420 [gr-qc].
[19] N. Yunes and X. Siemens, Living Reviews in Relativity **16**, 9 (2013), arXiv:1304.3473 [gr-qc].
[20] B. S. Sathyaprakash and B. F. Schutz, Living Reviews in Relativity **12**, 2 (2009), arXiv:0903.0338 [gr-qc].
[21] C. P. L. Berry, I. Mandel, H. Middleton, L. P. Singer, A. L. Urban, A. Vecchio, S. Vitale, K. Cannon, B. Farr, W. M. Farr, P. B. Graff, C. Hanna, C.-J. Haster, S. Mohapatra, C. Pankow, L. R. Price, T. Sidery, and J. Veitch, Astrophys. J. **804**, 114 (2015), arXiv:1411.6934 [astro-ph.HE].
[22] M. Isi, A. J. Weinstein, C. Mead, and M. Pitkin, Phys. Rev. D **91**, 082002 (2015), arXiv:1502.00333 [gr-qc].
[23] S. Dall'Osso, B. Giacomazzo, R. Perna, and L. Stella, Astrophys. J. **798**, 25 (2015), arXiv:1408.0013 [astro-ph.HE].
[24] L. De Vittori, A. Gopakumar, A. Gupta, and P. Jetzer, Phys. Rev. D **90**, 124066 (2014), arXiv:1410.6311 [gr-qc].
[25] W. E. East, Astrophys. J. **795**, 135 (2014), arXiv:1408.1695 [gr-qc].
[26] L. Wade, J. D. E. Creighton, E. Ochsner, B. D. Lackey, B. F. Farr, T. B. Littenberg, and V. Raymond, Phys. Rev. D **89**, 103012 (2014), arXiv:1402.5156 [gr-qc].
[27] J. Aasi, J. Abadie, B. P. Abbott, R. Abbott, T. D. Abbott, M. Abernathy, T. Accadia, F. Acernese, C. Adams, T. Adams, and et al., Phys. Rev. D **87**, 042001 (2013), arXiv:1207.7176 [gr-qc].
[28] J. Abadie, B. P. Abbott, R. Abbott, T. D. Abbott, M. Abernathy, T. Accadia, F. Acernese, C. Adams, R. Adhikari, C. Affeldt, and et al., Phys. Rev. D **85**, 122001 (2012), arXiv:1112.5004 [gr-qc].
[29] J. Abadie, B. P. Abbott, R. Abbott, M. Abernathy, T. Accadia, F. Acernese, C. Adams, R. Adhikari, P. Ajith, B. Allen, and et al., Classical and Quantum Gravity **27**, 173001 (2010), arXiv:1003.2480 [astro-ph.HE].
[30] M. Agathos, J. Meidam, W. Del Pozzo, T. G. F. Li, M. Tompitak, J. Veitch, S. Vitale, and C. Van Den Broeck, ArXiv e-prints (2015), arXiv:1503.05405 [gr-qc].
[31] B. D. Lackey and L. Wade, Phys. Rev. D **91**, 043002 (2015), arXiv:1410.8866 [gr-qc].
[32] K. Hotokezaka, K. Kyutoku, H. Okawa, and M. Shibata, Phys. Rev. D **91**, 064060 (2015), arXiv:1502.03457 [gr-qc].
[33] A. Maselli, L. Gualtieri, and V. Ferrari, Phys. Rev. D **88**, 104040 (2013), arXiv:1310.5381 [gr-qc].
[34] P. T. Baker, S. Caudill, K. A. Hodge, D. Talukder, C. Capano, and N. J. Cornish, Phys. Rev. D **91**, 062004 (2015), arXiv:1412.6479 [gr-qc].
[35] The LIGO Scientific Collaboration, J. Aasi, B. P. Abbott, R. Abbott, T. Abbott, M. R. Abernathy, K. Ackley, C. Adams, T. Adams, P. Addesso, and et al.,

Classical and Quantum Gravity **32**, 074001 (2015), arXiv:1411.4547 [gr-qc].
[36] J. Miller, L. Barsotti, S. Vitale, P. Fritschel, M. Evans, and D. Sigg, Phys. Rev. D **91**, 062005 (2015), arXiv:1410.5882 [gr-qc].
[37] C. L. Rodriguez, B. Farr, V. Raymond, W. M. Farr, T. B. Littenberg, D. Fazi, and V. Kalogera, Astrophys. J. **784**, 119 (2014), arXiv:1309.3273 [astro-ph.HE].
[38] Y. Aso, Y. Michimura, K. Somiya, M. Ando, O. Miyakawa, T. Sekiguchi, D. Tatsumi, and H. Yamamoto, Phys. Rev. D **88**, 043007 (2013), arXiv:1306.6747 [gr-qc].
[39] B. P. Abbott, R. Abbott, R. Adhikari, P. Ajith, B. Allen, G. Allen, R. S. Amin, S. B. Anderson, W. G. Anderson, M. A. Arain, and et al., Reports on Progress in Physics **72**, 076901 (2009), arXiv:0711.3041 [gr-qc].
[40] I. Mandel, C.-J. Haster, M. Dominik, and K. Belczynski, MNRAS **450**, L85 (2015), arXiv:1503.03172 [astro-ph.HE].
[41] T. B. Littenberg and N. J. Cornish, Phys. Rev. D **91**, 084034 (2015), arXiv:1410.3852 [gr-qc].
[42] C. Van Den Broeck, for the LIGO Scientific Collaboration, and the Virgo Collaboration, ArXiv e-prints (2015), arXiv:1505.04621 [gr-qc].
[43] G. Hammond, S. Hild, and M. Pitkin, Journal of Modern Optics **61**, 10 (2014), arXiv:1402.4616 [astro-ph.IM].
[44] B. Allen, W. G. Anderson, P. R. Brady, D. A. Brown, and J. D. E. Creighton, Phys. Rev. D **85**, 122006 (2012), gr-qc/0509116.
[45] M. Hannam, P. Schmidt, A. Bohé, L. Haegel, S. Husa, F. Ohme, G. Pratten, and M. Pürrer, Physical Review Letters **113**, 151101 (2014), arXiv:1308.3271 [gr-qc].
[46] P. Ajith, M. Hannam, S. Husa, Y. Chen, B. Brügmann, N. Dorband, D. Müller, F. Ohme, D. Pollney, C. Reisswig, L. Santamaría, and J. Seiler, Physical Review Letters **106**, 241101 (2011), arXiv:0909.2867 [gr-qc].
[47] K. Yagi, L. C. Stein, N. Yunes, and T. Tanaka, Phys. Rev. D **87**, 084058 (2013), arXiv:1302.1918 [gr-qc].
[48] N. Yunes, P. Pani, and V. Cardoso, Phys. Rev. D **85**, 102003 (2012), arXiv:1112.3351 [gr-qc].
[49] J. Gair and N. Yunes, Phys. Rev. D **84**, 064016 (2011), arXiv:1106.6313 [gr-qc].
[50] `LALSuite`, `https://www.lsc-group.phys.uwm.edu/daswg/projects/lalsuite.html` (2014).
[51] M. Coughlin, P. Meyers, E. Thrane, J. Luo, and N. Christensen, Phys. Rev. D **91**, 063004 (2015), arXiv:1412.4665 [gr-qc].
[52] T. Dal Canton, A. H. Nitz, A. P. Lundgren, A. B. Nielsen, D. A. Brown, T. Dent, I. W. Harry, B. Krishnan, A. J. Miller, K. Wette, K. Wiesner, and J. L. Willis, Phys. Rev. D **90**, 082004 (2014), arXiv:1405.6731 [gr-qc].
[53] K. A. Postnov and L. R. Yungelson, Living Reviews in Relativity **17**, 3 (2014), arXiv:1403.4754 [astro-ph.HE].
[54] L. Santamaría, F. Ohme, P. Ajith, B. Brügmann, N. Dorband, M. Hannam, S. Husa, P. Mösta, D. Pollney, C. Reisswig, E. L. Robinson, J. Seiler, and B. Krishnan, Phys. Rev. D **82**, 064016 (2010), arXiv:1005.3306 [gr-qc].
[55] P. Schmidt, M. Hannam, and S. Husa, Phys. Rev. D **86**, 104063 (2012), arXiv:1207.3088 [gr-qc].
[56] P. Ajith, M. Boyle, D. A. Brown, B. Brügmann, L. T. Buchman, L. Cadonati, M. Campanelli, T. Chu, Z. B. Etienne, S. Fairhurst, M. Hannam, J. Healy, I. Hinder, S. Husa, L. E. Kidder, B. Krishnan, P. Laguna, Y. T. Liu, L. London, C. O. Lousto, G. Lovelace, I. MacDonald, P. Marronetti, S. Mohapatra, P. Mösta, D. Müller, B. C. Mundim, H. Nakano, F. Ohme, V. Paschalidis, L. Pekowsky, D. Pollney, H. P. Pfeiffer, M. Ponce, M. Pürrer, G. Reifenberger, C. Reisswig, L. Santamaría, M. A. Scheel, S. L. Shapiro, D. Shoemaker, C. F. Sopuerta, U. Sperhake, B. Szilágyi, N. W. Taylor, W. Tichy, P. Tsatsin, and Y. Zlochower, Classical and Quantum Gravity **29**, 124001 (2012), arXiv:1201.5319 [gr-qc].
[57] F. Ohme, M. Hannam, and S. Husa, Phys. Rev. D **84**, 064029 (2011), arXiv:1107.0996 [gr-qc].
[58] T. Damour, P. Jaranowski, and G. Schäfer, Phys. Rev. D **63**, 044021 (2001), gr-qc/0010040.
[59] T. Damour, B. R. Iyer, and B. S. Sathyaprakash, Phys. Rev. D **63**, 044023 (2001), gr-qc/0010009.
[60] T. Damour, B. R. Iyer, and B. S. Sathyaprakash, Phys. Rev. D **66**, 027502 (2002), gr-qc/0207021.
[61] K. G. Arun, B. R. Iyer, B. S. Sathyaprakash, and P. A. Sundararajan, Phys. Rev. D **71**, 084008 (2005), gr-qc/0411146.
[62] B. Brügmann, J. A. González, M. Hannam, S. Husa, U. Sperhake, and W. Tichy, Phys. Rev. D **77**, 024027 (2008), gr-qc/0610128.
[63] S. Husa, M. Hannam, J. A. González, U. Sperhake, and B. Brügmann, Phys. Rev. D **77**, 044037 (2008), arXiv:0706.0904 [gr-qc].
[64] E. Berti, V. Cardoso, and C. M. Will, Phys. Rev. D **73**, 064030 (2006), gr-qc/0512160.
[65] D. Pollney, C. Reisswig, E. Schnetter, N. Dorband, and P. Diener, Phys. Rev. D **83**, 044045 (2011), arXiv:0910.3803 [gr-qc].
[66] P. D. Scharre and C. M. Will, Phys. Rev. D **65**, 042002 (2002), gr-qc/0109044.
[67] C. M. Will, Phys. Rev. D **50**, 6058 (1994), gr-qc/9406022.
[68] C. M. Will and N. Yunes, Classical and Quantum Gravity **21**, 4367 (2004), gr-qc/0403100.
[69] C. Brans", Physical Review **124**, 925 (1961).
[70] N. Cornish, L. Sampson, N. Yunes, and F. Pretorius, Phys. Rev. D **84**, 062003 (2011), arXiv:1105.2088 [gr-qc].
[71] E. Berti, A. Buonanno, and C. M. Will, Classical and Quantum Gravity **22**, 943 (2005), gr-qc/0504017.
[72] K. Yagi", Physical Review D **81** (2010), 10.1103/PhysRevD.81.064008.
[73] B. Bertotti, L. Iess, and P. Tortora, Nature **425**, 374 (2003).
[74] J. Veitch and A. Vecchio, Classical and Quantum Gravity **25**, 184010 (2008), arXiv:0807.4483 [gr-qc].
[75] B. Aylott, J. Veitch, and A. Vecchio, Classical and Quantum Gravity **26**, 114011 (2009).
[76] R. Umstätter and M. Tinto, Phys. Rev. D **77**, 082002 (2008), arXiv:0712.1030 [gr-qc].
[77] J. Clark, I. S. Heng, M. Pitkin, and G. Woan, Phys. Rev. D **76**, 043003 (2007), gr-qc/0703138.
[78] A. C. Searle, P. J. Sutton, and M. Tinto, Classical and Quantum Gravity **26**, 155017 (2009), arXiv:0809.2809 [gr-qc].
[79] S. Taylor, J. Ellis, and J. Gair, Phys. Rev. D **90**, 104028 (2014), arXiv:1406.5224 [gr-qc].
[80] X. Deng, Phys. Rev. D **90**, 104029 (2014), arXiv:1410.6441 [astro-ph.IM].
[81] J. Veitch, V. Raymond, B. Farr, W. Farr, P. Graff, S. Vitale, B. Aylott, K. Blackburn, N. Christensen, M. Coughlin, W. Del Pozzo, F. Feroz, J. Gair, C.-J. Haster, V. Kalogera, T. Littenberg, I. Mandel,

R. O'Shaughnessy, M. Pitkin, C. Rodriguez, C. Röver, T. Sidery, R. Smith, M. Van Der Sluys, A. Vecchio, W. Vousden, and L. Wade, Phys. Rev. D **91**, 042003 (2015), arXiv:1409.7215 [gr-qc].

[82] C. Kalaghatgi, P. Ajith, and K. G. Arun, Phys. Rev. D **91**, 124042 (2015), arXiv:1501.04418 [gr-qc].

[83] H.-S. Cho, ArXiv e-prints (2015), arXiv:1506.02745 [gr-qc].

[84] M. Dotti, A. Sesana, and R. Decarli, Advances in Astronomy **2012**, 940568 (2012), arXiv:1111.0664.

[85] H. Middleton, W. Del Pozzo, W. M. Farr, A. Sesana, and A. Vecchio, ArXiv e-prints (2015), arXiv:1507.00992.